frontiers | Frontiers in Environmental Science

TYPE Original Research
PUBLISHED 19 April 2024
DOI 10.3389/fenvs.2024.1379665

OPEN ACCESS

EDITED BY
Peiyue Li,
Chang'an University, China

REVIEWED BY
Hewen Niu,
Chinese Academy of Sciences (CAS), China
Dong-Hun Kim,
Korea Institute of Geoscience and Mineral Resources, Republic of Korea

*CORRESPONDENCE
Rui Wang,
wangr@igsnrr.ac.cn

RECEIVED 31 January 2024
ACCEPTED 03 April 2024
PUBLISHED 19 April 2024

CITATION
Cheng Y, Wang R, Liu Z and Yao Z (2024), Chemical weathering in the upper and middle reaches of Yarlung Tsangpo River.
Front. Environ. Sci. 12:1379665.
doi: 10.3389/fenvs.2024.1379665

Chemical weathering in the upper and middle reaches of Yarlung Tsangpo River

Yu Cheng[1,2], Rui Wang[1]*, Zhaofei Liu[1] and Zhijun Yao[1]

[1]Key Lab for Resources Use and Environmental Remediation, Institute of Geographic Sciences and Natural Resources Research, Chinese Academy of Sciences, Beijing, China, [2]College of Resources and Environment, University of Chinese Academy of Sciences, Beijing, China

This study focused on the chemical composition of the rivers in the middle and upper reaches of the Yarlung Tsangpo River system. Samples were collected in April 2015 to analyze spatiotemporal variation characteristics and determine weathering processes and CO_2 consumption using principal component analysis (PCA) and a modified forward model. The TDS on the southern bank of the upper and middle reaches of the Yarlung Tsangpo basin was found to be higher than that on the northern bank because of the difference in stratigraphic structure. The results show that the chemical facies of the rivers all belonged to Ca-HCO_3, and the rate of sulfuric acid-dominated chemical weathering was extremely high in the sub-watershed by $TZ^{+\square}/HCO_3^{-\square}$. Four major reservoirs (precipitation, silicates, carbonates, and evaporites) produce ions. The results of the chemical budget show that their contribution rates were 7.80% vs. 5.09% (PCA vs. modified forward model, the same below): 21.8% vs. 24.7%, 42.80% vs. 50.22%, and 10.30% vs. 21.59%, respectively. The ionic components from carbonate weathering in the study area were dominant, which is the main reason why the calculated results of the carbonate weathering rate (CWR) were higher than the silicate weathering rate (SWR). The CWR reached its maximum value during the monsoon period, whereas the SWR showed the opposite trend. Moreover, CO_2 sequestration by chemical weathering of rivers might be the main carbon sink in Tibet, which contributes to the realization of carbon neutrality in Tibet.

KEYWORDS

Yarlung Tsangpo River, chemical weathering, hydrochemistry, Tibetan Plateau, carbon dioxide absorption

1 Introduction

Owing to its unique plateau climate, the Qinghai–Tibet Plateau is very sensitive to global climate change and human activities; therefore, it has always been a hot spot of global climate change (Jia et al., 2019; Lu et al., 2020; Yang et al., 2023). The Yarlung Tsangpo River Basin is the largest and most important source of water in Tibet (W. Jiang et al., 2023). The study of the hydrochemistry of the Yarlung Tsangpo River and its tributaries can reveal the chemical evolution and main controlling factors of water in Tibet, which is helpful for deepening the understanding of the hydrochemical cycle in the Tibetan Plateau.

In the middle of the 20th century, European scientists initially established the river hydrochemical system, and their primary goal was to understand the relationships in rivers between natural geology and the sources of major ions, including K^+, Na^+, Ca^{2+}, Mg^{2+}, Cl^-, HCO_3^-, and SO_4^{2-}, as well as the composition ratios of various ions (Livingstone, 1963; Dawdy and Feth, 1967). Gibbs studied the chemical composition (mainly in ion ratio differences) of the main solutes of several rivers and classified the natural solutes of river

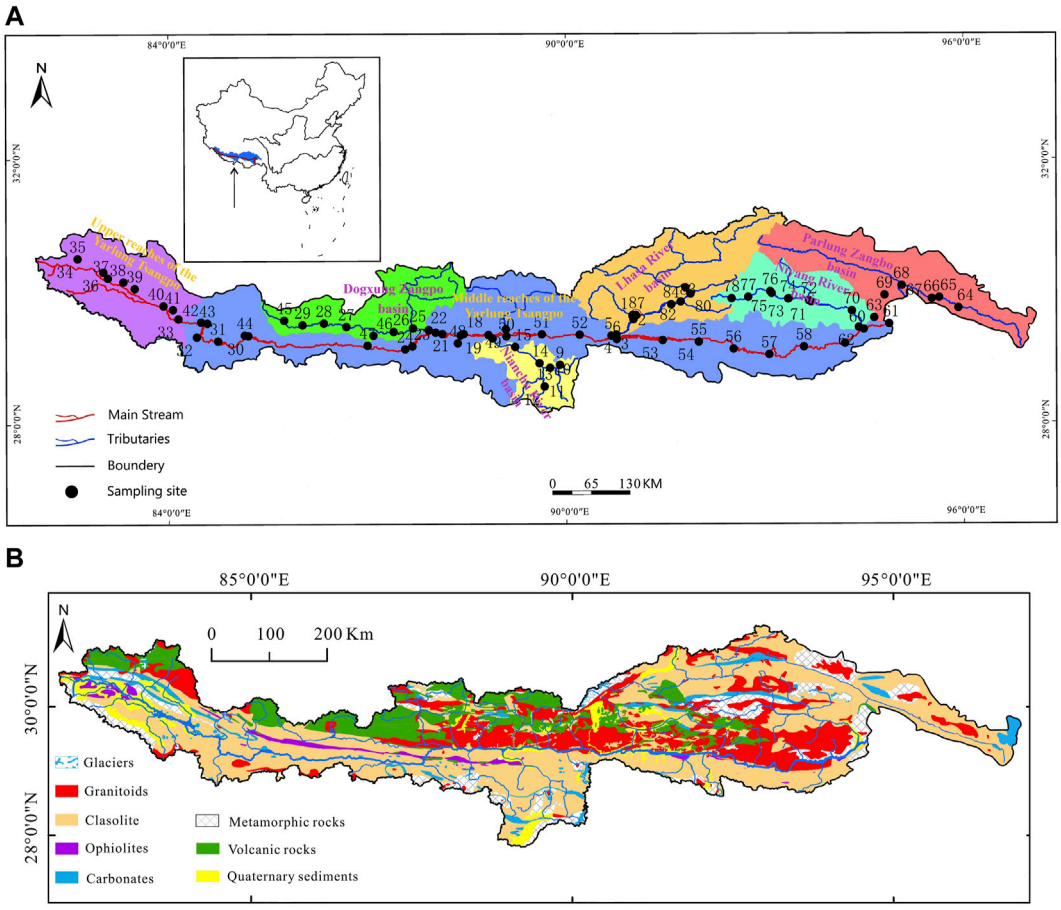

FIGURE 1
(A) Location of the UMRYT and its tributaries basins, with the sampling sites of this study. **(B)** Geologic map of the UMRYT basin (revised from Yu and China Geological Survey).

water into rock dominance, evaporation/crystallization dominance, and precipitation controlled, making a theoretical summary of the sources of solutes in natural rivers (Gibbs, 1971).

Chemical weathering affects the carbon cycle by absorbing CO_2 from the atmosphere and storing it in weathering products or mineralized marine sediments (Goudie and Viles, 2012). Although a link between chemical weathering and the carbon cycle on a global scale has been proposed since the 19th century, their relationship remains controversial (Chamberlin, 1899; Goudie and Viles, 2012). Some scientists have suggested that the uplift of the Tibetan Plateau during the Cenozoic accelerated chemical weathering, leading to a reduction in the atmospheric CO_2 content, which in turn contributed to global cooling during this period (Raymo and Ruddiman, 1992; Geng et al., 2023). This widely circulated hypothesis has led to the Tibetan Plateau and other orogenic belts becoming the focus of chemical weathering research in recent years (Ren et al., 2020; Geng et al., 2023).

The bedrock on the northern bank of the main stream is mainly composed of granitoids and volcanic rocks (Lhasa terrane) (Chamberlin, 1899), while the bedrock on the southern bank is mainly composed of clastic rocks and carbonates (Tethys sedimentary sequence, TSS) (Ma et al., 2022; Gao et al., 2023; Han et al., 2023). The significant spatial variation in the geographical environment within the watershed provides an ideal environment for studying chemical weathering processes and their intensities and controlling factors in the sub-watershed located in the southern Qinghai–Tibet Plateau (Goudie and Viles, 2012; Yu et al., 2021; Geng et al., 2023). However, there are some differences in the conclusions of different studies. Guan concluded that solute dissolution in the basin was low (Guan et al., 1984); Hren found low rates of chemical weathering and CO_2 consumption in most of the southern region, which was attributed to the low rates of precipitation and erosion in the region (Hren et al., 2007). However, Jiang concluded that CO_2 consumption caused by chemical weathering of silicates and carbonates significantly contributed to global CO_2 consumption (Chamberlin, 1899), while the results of Yu are exactly opposite to Jiang, suggesting that the rate of the chemical weathering and CO_2 consumption in the middle and upper reaches of the Yarlung Tsangpo River basin were almost the lowest in the world (Yu et al., 2021).

To analyze the accuracy of the above hypothesis, a detailed hydrochemical survey was conducted in April 2015 to evaluate the process and intensity of chemical denudation in the upper and middle reaches of the Yarlung Tsangpo River (UMRYT) and its subbasin. The modified forward model (Yu et al., 2021) was used to quantitatively calculate the proportion of chemical weathering in the basin, decipher the contribution of river solutes from different

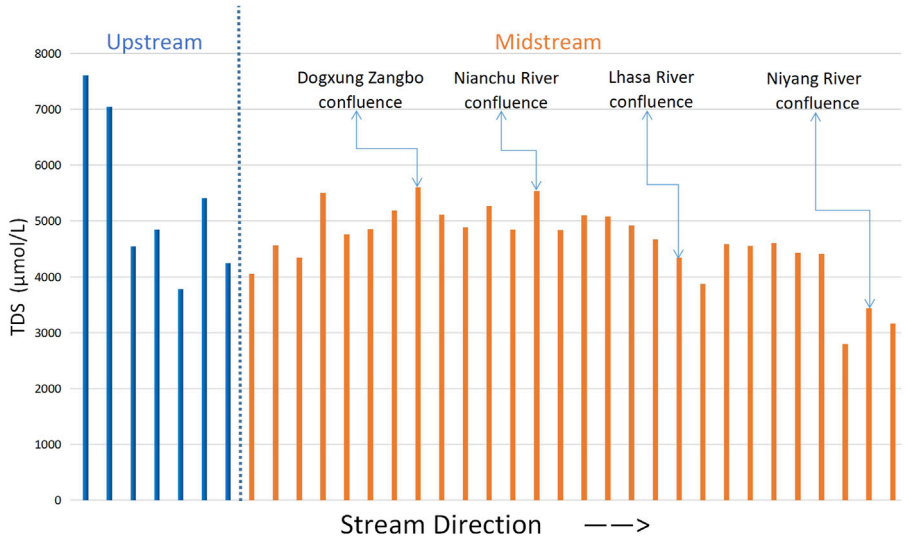

FIGURE 2
Variation in TDS along the main stream.

sources, and determine the geochemical process of hydrochemistry in the study area. The results were verified using principal component analysis (Pearson, 1901; Hotelling, 1933), and the rate of CO_2 consumption was calculated to test the correctness of the hypothesis above. The data were compared with the total carbon emission data of Tibet in 2014 and 2015 to evaluate the contribution of river chemical weathering sequestration of CO_2 to regional carbon neutrality.

2 Materials and methods

The Yarlung Tsangpo River Basin is the most important source of water resources in Tibet. The river originates from the northern slope of the central Himalayas, flows from west to east, turns southward, and finally flows into India in the Luoyu region (Guo et al., 2023; L. G. Jiang et al., 2015). The study area of this paper is in the middle and upper reaches of the Yarlung Tsangpo River, with its geographical location of 27° 48′–31° 18′ N and 85° 18′–112° 24′ E, covering an area about 216,000 km^2, and its elevation ranges from 3,543 to 7,068 m, 4,878.5 m on average (Bao, 2019; Bao et al., 2023; W. J. Liu et al., 2022; Lyu et al., 2023). The Indian Ocean monsoon is weakened in the region by the resistance of the Himalaya Mountains, so while the study area is located in a plateau region with intense radiation and long sunshine, the total accumulated heat is low, making the average temperature in the hottest month ranging from 11.2°C to 17.0°C, and the temperature of the coldest month below 0°C (Guo et al., 2023; Hu et al., 2022; W. J. Liu et al., 2022; Yu et al., 2021).

2.1 Geological setting

The strata in the study area are well-developed in all ages with various sedimentary types, the strata are well exposed, and fossils are abundant, especially from the Mesozoic period (Y. P. Feng et al., 2020; Ma et al., 2022). The southern side of the main stream is the Himalayan tectonic belt. The boundaries of the northern and southern tectonic belts are as follows: the Yarlung Tsangpo suture zone and main boundary collision fault are in the south, which are composed of the Precambrian metamorphic basement, overlying the Indian plate, and the sedimentary cap assemblage of the same period. The northern part of the belt is mainly composed of sedimentary caps, whose orientation is near east to west, and is composed of a set of Paleozoic and Mesozoic continental margin deposits, known as the TSS, see Figure 1A (J. L. Feng et al., 2017; Y. P. Feng et al., 2020). In the south, the Precambrian metamorphic basement is mainly composed of a set of highly deformed middle and deep metamorphic rocks that constitute the main body of the Himalayan tectonic belt. In the study area, the Nianchu River, Dogxung Zangbo, and Parlung Zangbo are located in the north of the Himalayan structural belt, and their underlying rocks are mostly clastic rocks, whereas the Lhasa and Niyang Rivers are located in the north of the middle and lower reaches of the main stream, and their underlying rocks are mostly volcanic rocks and granites (Goudie and Viles, 2012; Hemingway et al., 2020). The locations of the basin of the UMRYT and its tributaries are shown in Figure 1A.

2.2 Sampling and analytical methods

70 samples were collected from the mainstream and tributaries of the UMRYT in April 2015, including 69 river samples, and a rain sample. The locations of the river samples are shown in Figure 1A.

When the middle part of the river could be reached by a bridge or boat, samples were collected from the middle channel. When they could not be reached, samples were collected at the edge of the rivers. Acid-washed low-density polyethylene bottles were used to collect approximately 1 L of water samples at a depth of 50–100 cm below the surface of the river.

For quantitative measurement of cations, two bottles of filtered water samples were stored in two clean PE bottles, one of which was

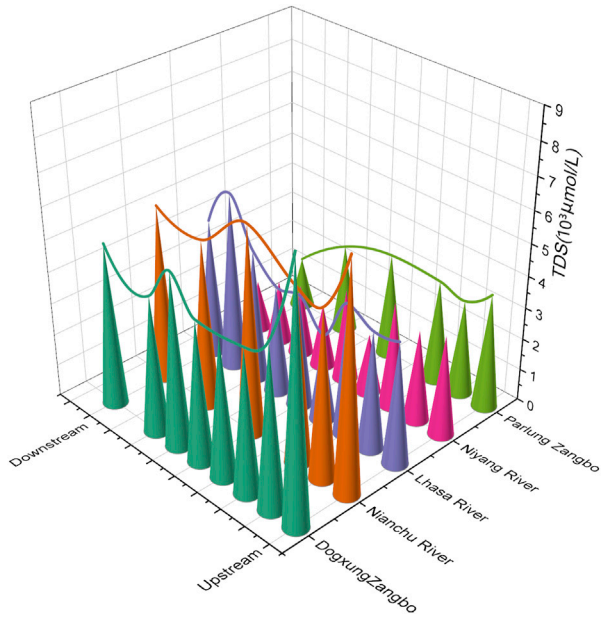

FIGURE 3
Changes in TDS along the tributaries.

acidified with three drops of 1:1 ultra-pure nitric acid to achieve <2 pH for cationic measurement. Samples from another bottle were used for anion testing. Major cations (K^+, Na^+, Ca^{2+}, and Mg^{2+}) were determined using inductively coupled plasma emission spectrometry (ICP-OES, Prodigy, Leeman) with a resolution of 0.001 mg/L. The major anions (Cl^-, NO_3^-, and SO_4^{2-}) were determined by ion chromatography (ICS-900, Dionex) with a resolution of 0.01 mg/L. Repeated measurements showed errors of ±2% for ICP-OES and ±5% for IC. HCO_3^- was calculated by titration.

3 Results

3.1 Spatial variation characteristics of hydrochemical ion components

By analyzing the spatial variation trend of TDS along the main stream (Figure 2), it was found that from the upper reaches to the end of the middle reaches of the Yarlung Tsangpo River, the TDS of the river first decreases (ends at the start of the middle reaches), then increases (ends when the Nianchu River influx), and finally decreases (until the end of the study area). By comparing the changes in TDS along the five tributaries (Figure 3), it was found that the values of TDS in the Lhasa and Niyang Rivers, which are on the north bank of the main stream, were relatively low. However, their values in the Nianchu River and Parlung Zangbo, which are on the south bank, were relatively high. The same applies to Dogxung Zangbo, which is on the north bank. Combined with the geological setting of the study area (Section 2.1), it was found that there was a very good coupling between the change rule of ion concentration in the river and the underlying layer.

By comparing the ratio of the ions, it was found that Ca^{2+} and HCO_3^- were the dominant anions and cations in the study area, respectively (Figure 4). In the upper reaches of the main stream, the proportion of HCO_3^- was in the range of 70%–80%, whereas in the middle reaches, the proportion was slightly reduced to approximately 70%. In the tributaries (Figure 5), the proportion of HCO_3^- in the Parlung Zangbo Basin was the highest (approximately 75%), slightly higher than in the Niyang, Lhasa, and Nianchu Rivers (the percentages in the three rivers were all about 70%), and the lowest appeared in the Dogxung Zangbo (approximately 65%). The proportion of $Ca^{2+}$and Mg^{2+} in the cation increased along the flow of the river. They increased from approximately 50% in the upper reaches to approximately 70% at the end of the middle reaches. In the tributaries, the proportion of $Ca^{2+}$and Mg^{2+} in Parlung Zangbo was the highest (approximately 85%), followed by the Nianchu, Lhasa, and Niyang Rivers (the percentages in the three rivers were all approximately 70%), and the lowest appeared in Dogxung Zangbo (only 55%).

The high proportions of $Ca^{2+}$and HCO_3^- indicate that carbonate dissolution is a common geochemical process in the UMRYT, and the dissolution of river ions is usually influenced by rock and mineral weathering, precipitation input, and human activities (Millot et al., 2002; Z. F. Zhou et al., 2023). Through analysis of the correlation and differences between ions, the influence of the above effects on the ionic type of the basin can be analyzed qualitatively and quantitatively.

3.2 Identification of chemical weathering processes

Chemical weathering refers to the process by which rocks change their chemical composition and form new substances under the influence of chemical factors such as water, CO_2, and O_2 as well as environmental factors such as temperature and wind (Jiang et al., 2015; Gao et al., 2023; Geng et al., 2023). The types of chemical weathering in the study area were determined by drawing a Gibbs diagram.

It was found that when using $Na^+/(Na^+ + Ca^{2+})$ or $Cl^-/(Cl^- + HCO_3^-)$ as indicators, the sampling projection points were all clustered in the rock dominance by drawing the Gibbs diagram (Figure 6), which confirms that the main composition of river ions in the study area tended to be dominated by rock weathering rather than dissolution of evaporative rocks in the surroundings or precipitation.

The Piper diagram (Figure 7) can be used to project water samples onto the grid by their ion concentration ratio, and the types of water can be judged by their position on the grid (Alqarawy, 2023). It was found that the type of all samples in the tributaries was Ca-HCO_3, the same as the main stream, which indicates that the chemical weathering in the study area was dominated by calcium bicarbonate. There was almost no difference in the proportion of anions in the tributaries of the right inferior anion triangle, whereas obvious differences in the ratio of Ca^{2+} were found in the left inferior cation triangle from high to low in Parlung Zangbo, Nianchu River, Niyang River, Lhasa River, and Dogxung Zangpo, indicating that the

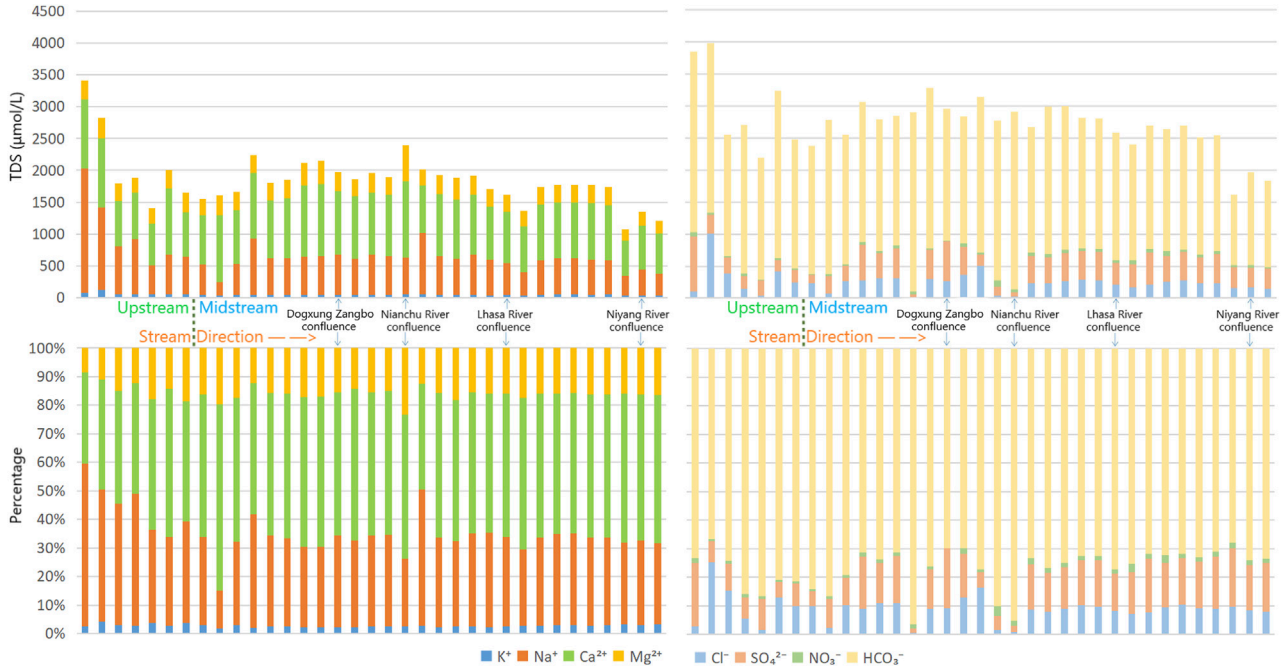

FIGURE 4
Changes of anion–cation along the main stream of Yarlung Tsangpo River.

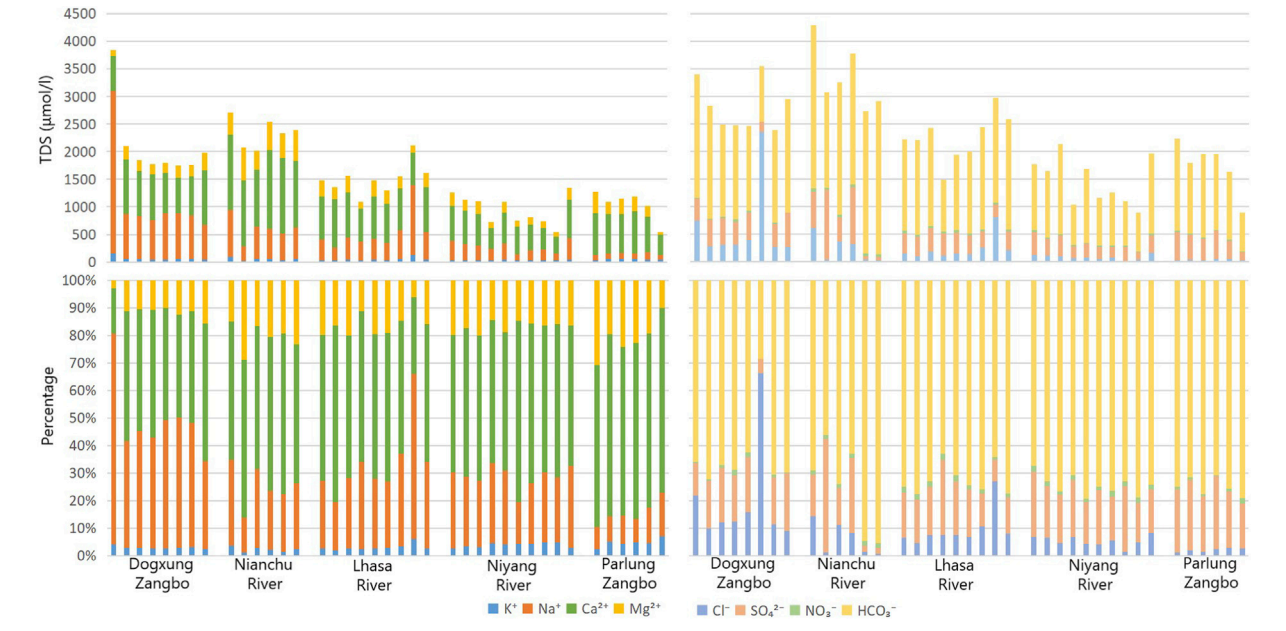

FIGURE 5
Changes in anion–cation along the tributaries.

types of chemical weathering among the tributaries were quite different.

The weathering of pyrite and weathering and dissolution of evaporite are the two main sources of sulfate in the rivers in the study area (Bao, 2019; Bao et al., 2023; L. G. Jiang et al., 2015). The influence of ions by sulfuric acid accounts for a large proportion of the chemical weathering in tributaries. Therefore, if all the SO_4^{2-} comes from the weathering of pyrite (mainly FeS), the projection of samples at the anion triangle in the piper diagram should be in the top left corner, but the result shows that they are at the bottom left, it could be concluded that the weathering and dissolution of evaporite were still the main source of SO_4^{2-}.

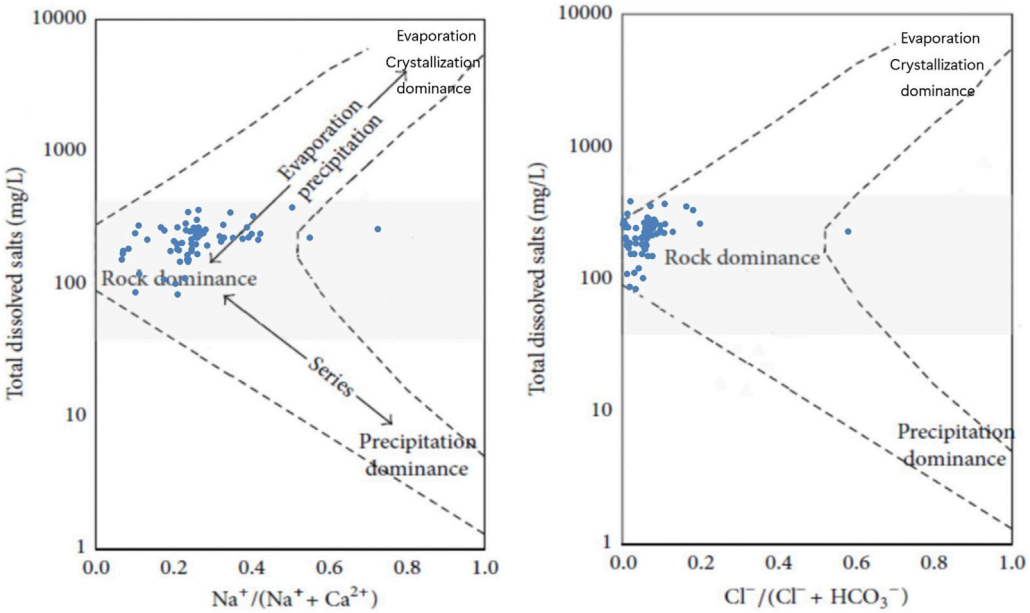

FIGURE 6
Gibbs diagram of rivers in the UMRYT.

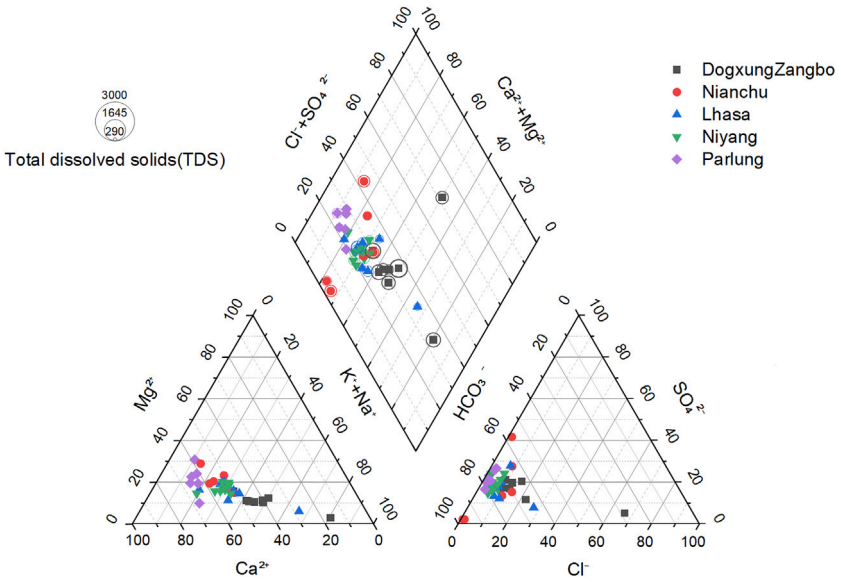

FIGURE 7
Piper diagram from each tributary.

The correlation coefficient reflects the source and connection of the ions. The Pearson correlation coefficient was calculated for the eight major ions in the study area (Table 1), finding that the pairwise correlation between K^+, Na^+, and SiO_2 was abnormally high (higher than 0.8), which indicates that the three ions were likely to have the same source. SiO_2 is almost completely derived from the weathering of silicate rocks; therefore, it can be inferred that the main source of the three ions was the dissolution of silicate rocks.

Moreover, the correlation coefficients between Ca^{2+}, Mg^{2+}, Ca^{2+}, and HCO_3^- were also very high (higher than 0.8). The correlation coefficient between Mg^{2+} and HCO_3^- was not low (0.69); therefore, it can be inferred that the main source of the three ions was probably the same. Combined with the stratigraphic and geographical information that calcium bicarbonate dominates chemical weathering in the study area, the main source of these three ions should be carbonate weathering.

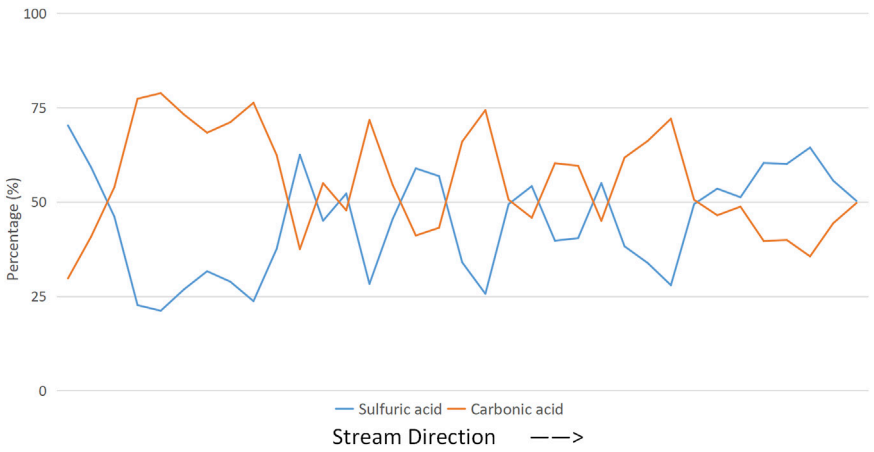

FIGURE 8
Variation in the main stream under the influence of the ratio of sulfuric and carbonate acids.

TABLE 1 Pearson correlation of the main ions.

	K^+	Na^+	Ca^{2+}	Mg^{2+}	Cl^-	SO_4^{2-}	NO_3^-	HCO_3^-
Na^+	0.828							
Ca^{2+}	0.166	0.238						
Mg^{2+}	−0.014	0.001	0.852					
Cl^-	0.453	0.454	0.075	−0.061				
SO_4^{2-}	0.023	0.145	0.366	0.338	−0.017			
NO_3^-	0.01	0.166	0.471	0.379	−0.155	0.139		
HCO_3^-	0.425	0.489	0.853	0.685	0.093	0.1	0.49	
SiO_2	0.812	0.878	0.074	−0.098	0.318	−0.002	0.025	0.334

TABLE 2 Average percentage of the influence of sulfuric and carbonic acids on tributaries.

Rivers	TZ^{+}* (mg/L)	HCO_3^-* (mg/L)	TZ^{+}*/HCO_3^-*	Influence of carbonic acid	Influence of sulfuric acid
Dogxung Zangbo	3.10	1.74	1.78	21.99%	78.01%
Nianchu River	4.09	2.47	1.65	34.51%	65.49%
Lhasa River	2.49	1.63	1.52	47.54%	52.46%
Niyang River	1.62	1.09	1.49	50.80%	49.20%
Parlung Zangbo	1.94	1.30	1.49	50.79%	49.21%
Average	3.03	2.11	1.44	56.06%	43.94%

As the influence of human effects on chemical weathering is minimal in the study area, HCO_3^- and SO_4^{2-} were extremely high in anions, and other ions such as $HNO_3^-$and Cl^- were in very small parts of the anion, it was deduced that the mixture of sulfuric acid and carbonic acid dominates regional weathering (Noh et al., 2009). To gain a better understanding of the trend of ion changes, it is necessary to understand the contribution ratio of sulfuric acid and carbonic acid to regional weathering.

According to the geological conditions of the study area (2.1), the underlying strata of the upper, middle upper, and southern banks of the UMRYT were TSS, which are mostly carbonate and silicate rocks. However, the middle lower reaches of the main stream and the northern bank of UMRYT were mostly affected by intrusive rock, mostly granite and volcanic rocks (Hemingway et al., 2020), and the dissolution reaction of carbonate and silicic rocks with carbonic or sulfuric acids would make the ratio between total cation

TABLE 3 The ratio between ions and Cl^-.

Ions/Ions	Cl^-/Cl^-	Na^+/Cl^-	Mg^{2+}/Cl^-	K^+/Cl^-	Ca^{2+}/Cl^-	NO_3^-/Cl^-	SO_4^{2-}/Cl^-	HCO_3^-/Cl^-
The ratio	1	0.91	0.8	0.63	5.05	0.43	0.47	23.89
TDS/Ions	TDS/Cl^-	TDS/Na^+	TDS/Mg^{2+}	TDS/K^+	TDS/Ca^{2+}	TDS/NO_3^-	TDS/SO_4^{2-}	TDS/HCO_3^-
The ratio	33.18	36.46	41.47	52.66	6.57	77.16	70.59	1.38

and SO_4^{2-}, and the ratio between total cation and HCO_3^- differ (Meybeck et al., 2003), so TZ^{+*}/SO_4^{2-*} and TZ^{+*}/HCO_3^{-*} were used to outline the carbonated and sulfuric acid-dominated chemical weathering reactions (Dawdy and Feth, 1967; Yu et al., 2021) (TZ^+ denotes the total cation, and * denotes the mass concentration, the same as below).

A high value of TZ^{+*}/SO_4^{2-*} indicates that chemical weathering in the area was dominated by sulfuric acid, and high values of TZ^{+*}/HCO_3^{-*} indicate that chemical weathering in the area was dominated by carbonic acid (Xuan et al., 2020). There are three possible sources of SO_4^{2-} in rivers: gypsum dissolution, sulfide oxidation, and anthropogenic input (Stachnik et al., 2016). However, because the study area is located in the interior of the Tibetan Plateau and belongs to the original environment, the influence of anthropogenic inputs on the concentration of sulfate ions was negligible. However, halides, evaporites, and sulfide minerals (mainly gypsum and pyrite) were found in the study area (Yan et al., 2022; J. W. Zhang et al., 2022; L. Zhou et al., 2022), so it is difficult to determine whether the main source of SO_4^{2-} in the river comes from evaporite dissolution (mainly hydrolysis of gypsum) or oxidation of sulfide (mainly pyrite). The exact source of SO_4^{2-*} cannot be determined, so it is impossible to use the index of TZ^{+*}/SO_4^{2-*} to calculate the influence of sulfuric and carbonic acids on regional weathering. Compared with SO_4^{2-}, after eliminating human disturbance and precipitation input, HCO_3^- in the study area was mainly (almost exclusively) derived from rock weathering; therefore, it was more reasonable and accurate to use TZ^{+*}/HCO_3^{-*} for analysis instead of TZ^{+*}/SO_4^{2-*}, and the calculation expression is as follows (Hindshaw et al., 2016):

Silicate weathering from carbonic acid:

$$TZ^{+*}/HCO_3^{-*} = 1; \quad (1)$$

Carbonate weathering from carbonic acid:

$$TZ^{+*}/HCO_3^{-*} = 1; \quad (2)$$

Silicate weathering from sulfuric acid:

$$TZ^{+*}/HCO_3^{-*} = \infty; \quad (3)$$

Carbonate weathering caused by sulfuric acid:

$$TZ^{+*}/HCO_3^{-*} = 2; \quad (4)$$

In the entire watershed, the average pH is 8.4, and the average pH of each tributary is close to 8, all of which are weakly alkaline. The evaporite dissolution of sulfuric acid (with a low concentration) preferentially reacts with carbonate rocks with more active properties than silicite rocks (Hindshaw et al., 2016). At the same time, the main area of weathering in the study area is the TSS, which is easily weathered and denuded on the south bank of the UMRYT, whose internal lithology is mostly carbonate rocks. Based on these two factors, the reaction between sulfuric acid and silicate rocks was ignored in the study area. According to Eqs 1–4, the percentage of influence of sulfuric and carbonic acids on rivers in the study area can be calculated. The calculation results are in Table 2.

The results show that the tributaries closer to the upstream were more affected by sulfuric acid, whereas the tributaries closer to the downstream were more affected by carbonic acid (Figure 8). The weathering of the mainstream in the entire study area was slightly more affected by carbonic acid than by sulfuric acid. Considering the stratigraphic information and the location of the watershed above, the phenomenon could be explained as follows: rivers flow fast and dangerously near the upstream, and a higher velocity makes sulfuric acid more likely to ionize instead of carbonate acid. Although the proportion of bicarbonate in the basin is more prominent, weak alkali conditions allow sulfuric acid to react first, which causes a stronger erosion of surrounding rocks. The underlying surface of the middle and lower reaches of the main streams is relatively flat, helping the velocity of the flow to slow down; thus, the rivers have more time to fully react with the surrounding carbonate rocks, making the carbonate erosion of the surrounding rocks stronger.

3.3 Contributions of chemical weathering

3.3.1 Hydrologic model method

There were six the main sources of ions in the study area, and they were as follows: precipitation, evaporation, oxidation of sulfide, silicate weathering, carbonate dissolution, and human activities (L. G. Jiang et al., 2015; Yan et al., 2022). The influence of human activities on chemical weathering in the study area was ignored because it was not significant. When calculating the contribution ratio of weathering, the modified forward model can be expressed as Eq. 5:

$$X_{riv} = X_{atm} + X_{eva} + X_{sul} + X_{sil} + X_{car} \quad (5)$$

where X represents cations, and the subscripts *riv*, *atm*, *eva*, *sul*, *sil*, and *car* represent cations in the river, atmospheric input, evaporite dissolution, sulfide oxidation, silicate weathering, and carbonate dissolution, respectively (see below).

The idea of the model is to cover all input ions; however, it is difficult to fully measure the data of each input term. To calculate various weathering results with limited data, the model simplifies and approximates the source of each ion (J. J. Liu and Guo, 2023; Yu et al., 2021). The results are as follows:

1) All Cl^- in rivers originated from evaporite dissolution after modified atmospheric input; 2) all Na^+ in the river originated from silicate weathering after modified atmospheric input and evaporite dissolution; and 3) all K^+ in the river originated from silicate

TABLE 4 Ion contribution of meteoric water to the river basin.

Ion concentration	K^+	Na^+	Ca^{2+}	Mg^{2+}	Cl^-	SO_4^{2-}	NO_3^-	HCO_3^-
Precipitation (μmol/L)	8.62	12.45	41.72	10.94	13.68	6.43	5.88	326.82
Rivers (μmol/L)	52.96	586.52	793.47	261.49	263.63	396.04	32.02	1,740.91
Percentage (%)	16.27	2.12	5.26	4.19	5.19	1.62	18.37	18.77

weathering after modified atmospheric input. 4) The correlation coefficient between SO_4^{2-} and Ca^{2+} (R^2 = 0.837) was significant, indicating that the source of the two ions may be from the dissolution of gypsum or carbonate, as well as sulfuric acid formed by the oxidation of sulfide. 5) Therefore, we assume that half of the SO_4^{2-} in river came from evaporite dissolution, which is more reasonable than assuming all SO_4^{2-} in river was from evaporation or sulfide oxidation (Yu et al., 2021).

After assuming the limitations above, the source of each ion in the river can be obtained as Eqs 6–11:

$$Cl_{riv}^- = Cl_{atm}^- + Cl_{eva}^- \tag{6}$$

$$SO_{4\ riv}^{2-} = SO_{4\ atm}^{2-} + SO_{4\ eva}^{2-} + SO_{4\ sul}^{2-} \tag{7}$$

$$K_{riv}^+ = K_{atm}^+ + K_{sil}^+ \tag{8}$$

$$Na_{riv}^+ = Na_{atm}^+ + Na_{eva}^+ + Na_{sil}^+ \tag{9}$$

$$Ca_{riv}^{2+} = Ca_{atm}^{2+} + Ca_{eva}^{2+} + Ca_{sil}^{2+} + Ca_{car}^{2+} \tag{10}$$

$$Mg_{riv}^{2+} = Mg_{atm}^{2+} + Mg_{sil}^{2+} + Mg_{car}^{2+} \tag{11}$$

At the same time, the equations for each weathering source can be expressed as Eqs 12–16 (denotes molar concentration, the same below):

$$X_{atm} = \left([K^+]_{atm} + [Na^+]_{atm} + 2[Ca^{2+}]_{atm} + 2[Mg^{2+}]_{atm}\right)/[TZ^+]_{riv} \tag{12}$$

$$X_{eva} = \left([Na^+]_{eva} + 2[Ca^{2+}]_{eva}\right)/[TZ^+]_{riv} \tag{13}$$

$$X_{sil} = \left([K^+]_{sil} + [Na^+]_{sil} + 2[Ca^{2+}]_{sil} + 2[Mg^{2+}]_{sil}\right)/[TZ^+]_{riv} \tag{14}$$

$$X_{car} = \left(2[Mg^{2+}]_{car} + 2[Ca^{2+}]_{car}\right)/[TZ^+]_{riv} \tag{15}$$

$$[TZ^+]_{riv} = [K^+]_{riv} + [Na^+]_{riv} + 2[Ca^{2+}]_{riv} + 2[Mg^{2+}]_{riv} \tag{16}$$

The source of Cl^- in rivers was relatively stable without the influence of human activities, and Cl^- will not react with other ions and form precipitates; therefore, the concentration of other ions in precipitation can be calculated by the ratio of Cl^-. The equations used are as Eqs 17, 18 Gaillardet et al. (1999):

$$X_{atm} = (X/Cl)_{rain} \times Cl_{min} \tag{17}$$

$$\text{And } X_{atm} = (X/Cl)_{rain} \times Cl_{ref} \tag{18}$$

where F denotes the evapotranspiration coefficient in $Cl_{ref} = Cl_{ave} \times F$, X_{atm} denotes the concentration of ions produced by precipitation, $(X/Cl)_{rain}$ denotes the molar concentration ratio of TDS to Cl^- in precipitation, and Cl_{min} denotes the minimum Cl^- in the river. The value of F in the study area is 1.41 during non-monsoon periods. Therefore, the value of Cl_{min} in April 2015 was 18.4 μmol/L. Using the relationship between the other ions and Cl^- (D. D. Zhang et al., 2003), which are shown in Table 3, the values of the other ions in precipitation can be calculated as shown in Table 4.

According to Moon and Noh, the concentrations of Ca^{2+} and Mg^{2+} imported from surface runoff weathered by silicate rocks (mainly anorthite) can be expressed as Eqs 19, 20 (Moon et al., 2007; Noh et al., 2009):

$$Ca_{sil}^{2+} = \left(Ca^{2+}/Na^+\right)_{sil} \times Na_{sil}^+ \tag{19}$$

$$Mg_{sil}^{2+} = \left(Mg^{2+}/K^+\right)_{sil} \times K_{sil}^+ \tag{20}$$

Theoretically, the values of $(Ca^{2+}/Na^+)_{sil}$ and $(Mg^{2+}/K^+)_{sil}$ should be the average everywhere in the river basins, but this is almost impossible when studying a large basin. Therefore, we chose to use the data of sand and rocks in the riverbed as an approximation for an alternative analysis (Wu, 2016). The values of $(Ca^{2+}/Na^+)_{sil}$ and $(Mg^{2+}/K^+)_{sil}$ in the study area were measured by electron probes based on 42 types of plagioclase particles, which were approximately 0.545 and 0.3, respectively (Booth et al., 2004; Hren et al., 2007).

The results showed that the average contribution of precipitation to the river ion concentration was approximately 5.09%, and the average proportions in the tributaries were in the order of the Niyang River (8.39%) > Parlung Zangbo (7.16%) > Lhasa River (5.16%) > Duxiong Zangpo (4.20%) > Nianchu River (3.11%), which is consistent with the spatial distribution of rainfall.

The average evaporite weathering was approximately 21.59%, and the average in the tributaries was in the order of Dogxung Zangbo (26.23%) > Lhasa River (22.68%) > Parlung Zangbo (20.71%) > Niyang River (20.25%) > Nianchu River (19.59%). A similar number of results indicates that evaporite weathering occurred over a wide and stable range in the study area. However, the results for Dogxung Zangbo were approximately 5% higher than the average of the other tributaries. In addition to the topographic effects mentioned above, this phenomenon also indicates that the dissolution of gypsum and halide is significant in Dogxung Zangbo.

The average contribution of silicate weathering to the river ion concentration was approximately 2 24.07%, and the average proportion in the tributaries was in the order of Dogxung Zangbo (35.05%) > Lhasa River (23.28%) ≈ Niyang River (23.02%) > Nianchu River (17.82%) > Parlung Zangbo (11.61%). The elevation of the water surface varied greatly in Dogxung Zangbo because its basin is in the upper reaches of the main stream; therefore, it has a good erosion effect on silicates that are relatively insoluble, making it the first in the tributaries. Meanwhile, Parlung Zangbo, which is in the same stratum as Dogxung Zangbo, had a relatively weak weathering effect on silicates because it is located downstream and the topography is relatively flat. The results for the Lhasa and Niyang Rivers were higher than those for the Nianchu River because of the difference in the underlying layers.

The average contribution of carbonate weathering to the river ion concentration was approximately 50.22%, and the average in the tributaries was in the order of Parlung Zangbo (60.52%) > Nianchu River (59.47%) > Lhasa River (48.88%) ≈ Niyang River (48.33%) >

TABLE 5 Accumulation of eigenvalues.

Eigenvalue	4.283	1.959	0.924	0.702	0.531	0.280	0.189	0.089	0.043
Ratio (%)	47.600	21.800	10.300	7.800	5.900	3.100	2.100	1.000	0.500
Accumulate (%)	47.600	69.400	79.600	87.400	93.300	96.400	98.500	99.500	100.000

TABLE 6 Matrix of score coefficients.

Variable	Factor 1	Factor 2	Factor 3	Factor 4
K^+	0.342	0.019	0.238	0.076
Na^+	0.247	0.139	0.273	0.132
Ca^{2+}	0.039	0.391	0.099	0.016
Mg^{2+}	0.124	0.479	0.187	0.046
Cl^-	0.305	0.032	0.220	0.158
SO_4^{2-}	0.006	0.137	0.007	0.960
NO_3^-	0.120	0.157	0.988	0.002
HCO_3^-	0.049	0.371	0.038	0.256
SiO_2	0.296	0.090	0.090	0.131

Dogxung Zangpo (34.09%). The rocks beneath Parlung Zangbo are mostly carbonate rocks, and the location of the river is around the middle and lower reaches of the main stream, helping it flow gently, which made the carbonate weathering very strong here. The ion concentrations from chemical weathering in Duoxiong Zangpo were higher than those in the Niyang and Lhasa Rivers, but a larger number of ions from other chemical weathering sources, which made the ratio of carbonate weathering relatively low.

3.3.2 Principal component analysis

Principal component analysis (PCA) (Pearson, 1901; Hotelling, 1933) is a statistical method that converts a set of potentially correlated variables into a set of linearly uncorrelated variables through orthogonal transformation and calculates the main influencing factors from the differences in the explained variance of each other. It treats the remaining unexplained factors, such as noise (or unimportant factors) (Bhatt and Maclean, 2023). Here, PCA was used to cluster the river ion concentrations and analyze the load of the principal component. The results of the control factors were the chemical weathering effects, which can be used to calculate and prove the contribution of different rock weathering processes to river solutes.

The accumulated eigenvalues of the factors were calculated as shown in Table 5. The first four principal components, whose cumulative variance contribution rate was approximately 87.4% (more than 85%), were selected and considered to have no loss of information. After factor analysis of the data and orthogonal rotation of the initial factors by Minitab, the score coefficient matrix (Table 6) and common factor variance matrix (Table 7) were obtained.

To better determine the actual physical significance of each factor, hierarchical cluster analysis (HCA) was used to make assumptions regarding the sources of ions observed in the rivers (J. J. Liu and Guo, 2023). The samples could be divided into different hydration groups according to the correlation between the ion concentrations (Figure 9). The ion concentration changes were similar in the same group, indicating that there may be similar provenances. Samples of the nine ions were divided into four main groups according to Figure 9: Group 1: Ca^{2+}, Mg^{2+}, and HCO_3^-; Group 2: Na^+, K^+, SiO_2, and Cl^-; Group 3: SO_4^{2-}; and Group 4: NO_3^-.

The variance contribution rate of the first factor was 41.80%, and it was mainly related to Ca^{2+}, Mg^{2+}, and HCO_3^- according to the score matrix table (Table 5), which were the main products of carbonate weathering; therefore, carbonate weathering is the first factor that influences the ion concentration in the basin. Similarly, the variance contribution rates of the second, third, and fourth factors were 27.20%, 10.50%, and 9.50%, respectively, which represent the weathering of silicate rock, evaporite, and precipitation, respectively. The results of the variance contribution rates here are similar to the results calculated by the modified forward model in 3.3.1, which proves the correctness of the model calculation results from a statistical perspective.

The North test (Deschasaux-Tanguy et al., 2021) is a significant test implemented by calculating the error range of the eigenvalue. The eigenvalues are denoted by λ, and their error range can be expressed as Eq. 21:

$$e_j = \lambda_j \left(\frac{2}{n}\right)^{\frac{1}{2}} \tag{21}$$

where n is the number of samples. When the adjacent eigenvalue λ_{j+1} meets $\lambda_j - \lambda_{j+1} \geq e_j$, the two empirical orthogonal functions are regarded as valuable, so the table of the results of the North test can be made as follows.

The four factors have passed the North test according to the test results in Table 8.

3.4 Rate of chemical weathering

The carbonate weathering rate (CWR) and silicate weathering rate (SWR) were calculated by combining the cationic components of carbonate and silicate with the velocity of runoff and catchment area as Eqs 22, 23 (Grasby et al., 2000).

$$SWR = \left([K]_{sil} + [Na]_{sil} + [Ca]_{sil} + [Mg]_{sil}\right) \times runoff / drainage\ area \tag{22}$$

$$CWR = \left(1/2\,[HCO_3^-]_{car} + [Ca]_{car} + [Mg]_{car}\right) \times runoff / drainage\ area \tag{23}$$

Hydrochemical data from the sampling site closest to the estuary were used to calculate the average rate of chemical denudation within the catchment. Therefore, 11 samples were selected from the estuaries of the five tributaries to represent the average values.

TABLE 7 Loadings and common factor variance.

Variable	Factor 1	Factor 2	Factor 3	Factor 4	Common factor variance
K^+	0.681	0.562	0.080	0.179	0.818
Na^+	0.831	0.363	0.034	0.221	0.872
Ca^{2+}	0.808	0.517	0.003	0.171	0.949
Mg^{2+}	0.625	0.682	0.035	0.260	0.925
Cl^-	0.637	0.434	0.262	0.089	0.670
SO_4^{2-}	0.364	0.386	0.780	0.301	0.980
NO_3^-	0.569	0.251	0.420	0.618	0.945
HCO_3^-	0.891	0.232	0.232	0.207	0.944
SiO_2	0.656	0.570	0.097	0.029	0.765
Variance	4.283	1.959	0.924	0.702	7.869
Variance contribution rate (%)	47.600	21.800	10.300	7.800	87.400

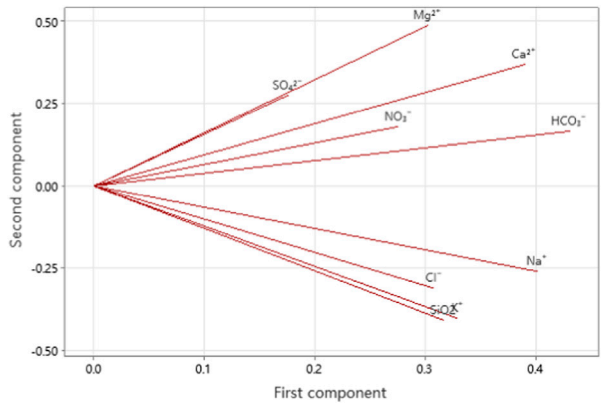

FIGURE 9
Ions loading.

The uncertainty factors in the study mainly originated from the uncertainty of the volume of runoff and cation concentration. Therefore, the error propagation equations were evaluated in this study, that is, $\sigma WR = \sqrt{(\sigma Q)^2 + (\sigma C)^2}$, where σWR indicates the transmission error of the chemical weathering rate, and σQ and σC indicate the volume of runoff and ion concentration error caused by measurements, respectively. The uncertainty of the chemical weathering rate in the study area was found to be less than ± 20% after the calculation.

The calculation results are compared with the results of other scholars in the same period in Table 9, which shows that the CWR data are lower but the (Berry et al., 2005) SWR data are relatively higher in the study than in the monsoon (summer), which is consistent with the natural conditions of rain heat synchronization in the study area.

There is no obvious difference between the SWR and CWR in the study area, while the large differences between the tributary strata indicate that carbonate and silicate weathering may be oversaturated, which may be limited by temperature, rainfall, and material conditions other than the region itself.

4 Discussion

Compared with the modified forward model, the PCA calculation results for the contribution rates of different weathering processes were mostly smaller. This is because the accumulated variance explanation rate of the first four principal components was only 87.4%, 12.6% of which was ignored as noise, including the influence of human factors. However, the contribution of the four chemical weathering effects was considered 100% in the modified forward model, making the calculation results higher.

The result of CO_2 absorption by the SWR was lower in this study than that reported by Yu. This is because the resistance to weathering in silicate rocks is stronger than that in carbonate rocks. Therefore, silicate weathering reacts more thoroughly than carbonate weathering at the low velocity of a large contact area, which is consistent with the fact that the flow velocity in the study area decreases significantly in winter. The Niyang River performed best in the SWR among the five tributaries because of its high flow rate, and its depth is 3–4 times more than that of the other tributaries, making it highly erosive. The underlying rocks of Parlung Zangbo are carbonate. The low flow velocity in a large contact area helped it rank first in CWR. However, the performance of the SWR in Parlung Zangbo was not as good as that in the Niyang River, indicating that the drainage basin may be oversaturated by chemical weathering. In other words, excessive weathering of carbonate rocks seized the reactant, which could react with silicate rocks due to oversaturation.

Global warming increases the rate of chemical weathering and glacial melt, but there is no clear evidence that it can increase global precipitation. Therefore, under the conditions of global warming, the rate of CO_2 absorption in the Yarlung Tsangpo River Basin will certainly increase before the decrease in water from the melting of the glacier. Yu et al. (2021) found that the amounts of CO_2 sequestration caused by chemical weathering of carbonate and silicate in the four tributaries (excluding the Parlung Zangbo basin) is about 34.70×10^9 mol/y by the samples collected in 2012 and 2013, while our study found that the annual carbon sequestration of the four tributaries is estimated to be 35.64×10^9 mol/y in 2015. Consistency across the two

TABLE 8 North test.

Modal sequences	Eigenvalue	Error range	Maximum eigenvalue of the lower mode
1	4.283	0.704	3.579
2	1.959	0.322	1.637
3	0.924	0.152	0.772
4	0.702	0.115	0.587
5	0.531	—	—

TABLE 9 Comparison between SWR and CWR.

Weathering type	Rivers	2012, 2013 Yu et al. (2021)	2015 (this study)	2016, 2017 Bao (2019)
CWR (t/km^2/y)	Dogxung Zangbo	12.6 ± 4.8	11.7 ± 3.0	6.48–44.88
	Nianchu River	15.8 ± 5.6	14.8 ± 3.1	
	Lhasa River	12.5 ± 3.0	13.5 ± 3.7	
	Niyang River	20.0 ± 5.8	13.5 ± 4.4	
	Parlung Zangbo	—	36.9 ± 4.1	—
SWR (t/km2/y)	Dogxung Zangbo	3.4	6.2 ± 0.9	1.8–10.92
	Nianchu River	2.9	4.6 ± 0.1	
	Lhasa River	4.0	4.8 ± 0.9	
	Niyang River	5.6	10.4 ± 3.2	
	Parlung Zangbo	—	4.9 ± 0.7	—

studies bolsters the credibility of our calculations and reaffirms the upward trajectory of CO_2 absorption trends.

Though the data from the CEADs (Shan et al., 2017) showed that the total carbon emissions (TCE) in the whole region of Tibet in 2014 was 5.518×10^9 kg, the figure is expected to rise to 35.73×10^9 kg in 2015 because of the massive output of natural gas (the carbon emissions caused by natural gas reached 29.073×10^9 kg in 2015 and no more than 1×10^9 kg in 2014). According to "the Plan of Tibet for the Control of Greenhouse Gas Emissions during the 13th Five-Year Plan Period," Tibet started saving energy and reducing emissions in 2015, and CO_2 emission intensity per unit of GDP was reduced by 12% in 2020, as compared with 2015. This suggests that the impact of human activities on carbon emissions in Tibet peaked in 2015 and is expected to gradually diminish in the foreseeable future. However, the annual carbon sequestration of the five tributaries is estimated to be about 62.38×10^9 mol/y, or 2.74467×10^9 kg/y, accounting for 49.7% of the TCE in 2014 and 7.7% of the TCE in 2015 in Tibet, underscoring the potential significance of river-based carbon sequestration as a vital CO_2 treatment sink (Yu et al., 2021; Bao et al., 2023). These findings suggest that river-based carbon sequestration could play a crucial role in achieving carbon neutrality objectives in Tibet.

5 Conclusion

The TDS along the main stream of the study area first decreased and then increased. The ion concentrations of the tributaries were in the order of Nianchu River > Dogxung Zangbo > Lhasa River > Niyang River ≈ Parlung Zangbo. The average TDS of the sampling sites located on the south bank of the main stream was higher than that on the north bank, and was mainly influenced by the underlying layer and different flow velocities in different regions. The hydrochemical type of river water in the study area was Ca-HCO_3. The two ions accounted for 62.4% of the total ion concentration on average, followed by Na^+, Mg^{2+}, and SO_4^{2-}; the weathering type in the study area was rock weathering, which was mainly controlled by sulfuric acid.

The results of the chemical budget calculation showed that the contribution rates of precipitation, silicate, carbonate, and evaporite weathering to the ionic components in the surface water of the study area were 7.80% vs. 5.09% (PCA vs. modified forward model, same below), 21.8% vs. 24.7%, 42.80% vs. 50.22%, and 10.30% vs. 21.59%, respectively. The contribution of carbonate weathering to the source of ion components in the study area was dominant, which was the main reason why the CWR results were higher than those of the SWR. The CWR reached its maximum value during the monsoon period, whereas the SWR showed the opposite trend. The values of the SWR in the tributaries showed that chemical weathering in the study area may be oversaturated. Carbon sequestration from rivers in Tibet has been an important sink for CO_2 treatment for decades, which makes a great contribution to the realization of carbon neutrality in Tibet. However, the phenomenon of carbon pollution in Tibet is insignificant, and the ecological capacity of carbon storage remains strong.

Data availability statement

The original contributions presented in the study are included in the article/Supplementary material, further inquiries can be directed to the corresponding author.

Author contributions

YC: Conceptualization, Data curation, Formal Analysis, Investigation, Methodology, Project administration, Software, Validation, Writing–original draft, Writing–review and editing. RW: Conceptualization, Data curation, Formal Analysis, Investigation, Methodology, Project administration, Writing–review and editing. ZL: Conceptualization, Data curation, Investigation, Methodology, Supervision, Validation, Writing–review and editing. ZY: Conceptualization, Data curation, Funding acquisition, Methodology, Resources, Supervision, Writing–review and editing.

Funding

The author(s) declare financial support was received for the research, authorship, and/or publication of this article. This work was supported and funded by the Strategic Priority Research Program of the Chinese Academy of Sciences (XDA23090302 and XDA2006020202).

Acknowledgments

We would like to thank all the contributors and the Frontiers staff who have made this research topic possible.

Conflict of interest

The authors declare that the research was conducted in the absence of any commercial or financial relationships that could be construed as a potential conflict of interest.

Publisher's note

All claims expressed in this article are solely those of the authors and do not necessarily represent those of their affiliated organizations, or those of the publisher, the editors and the reviewers. Any product that may be evaluated in this article, or claim that may be made by its manufacturer, is not guaranteed or endorsed by the publisher.

References

Alqarawy, A. (2023). Assessment of shallow groundwater aquifer in an arid environment, Western Saudi Arabia. *J. Afr. Earth Sci.* 200, 104864. doi:10.1016/j.jafrearsci.2023.104864

Bao, Y. F. (2019). *The study of hydrochemical characteristics and carbon cycles in the Yarlung Zangbo Basin*. China Institute of Water Resources and Hydropower Research.

Bao, Y. F., Hu, M. M., Li, S. Z., Wang, Y. C., Wen, J., Wu, X. H., et al. (2023). Carbon dioxide partial pressures and emissions of the Yarlung Tsangpo River on the Tibetan plateau. *Front. Environ. Sci.* 10. doi:10.3389/fenvs.2022.1036725

Berry, P. A. M., Garlick, J. D., Freeman, J. A., and Mathers, E. L. (2005). Global inland water monitoring from multi-mission altimetry. *Geophys. Res. Lett.* 32 (16). doi:10.1029/2005gl022814

Bhatt, P., and Maclean, A. L. (2023). Comparison of high-resolution NAIP and unmanned aerial vehicle (UAV) imagery for natural vegetation communities classification using machine learning approaches. *Giscience Remote Sens.* 60 (1). doi:10.1080/15481603.2023.2177448

Booth, A. L., Zeitler, P. K., Kidd, W. S. F., Wooden, J., Liu, Y. P., Idleman, B., et al. (2004). U-Pb zircon constraints on the tectonic evolution of southeastern Tibet, Namche Barwa area. *Am. J. Sci.* 304 (10), 889–929. doi:10.2475/ajs.304.10.889

Chamberlin, T. C. (1899). Lord kelvin's address on the age of the earth as an abode fitted for life. II. *Science* 10 (236), 11–18. doi:10.1126/science.10.236.11

Dawdy, D. R., and Feth, J. H. (1967). Applications of factor analysis in study of chemistry of groundwater quality, Mojave River Valley, California. *Water Resour. Res.* 3 (2), 505–510. doi:10.1029/wr003i002p00505

Deschasaux-Tanguy, M., Druesne-Pecollo, N., Esseddik, Y., de Edelenyi, F. S., Alles, B., Andreeva, V. A., et al. (2021). Diet and physical activity during the coronavirus disease 2019 (COVID-19) lockdown (March-May 2020): results from the French NutriNet-Sante cohort study. *Am. J. Clin. Nutr.* 113 (4), 924–938. doi:10.1093/ajcn/nqaa336

Feng, J. L., Chen, F., and Hu, H. P. (2017). Isotopic study of the source and cycle of sulfur in the Yamdrok Tso basin, Southern Tibet, China. *Appl. Geochem.* 85, 61–72. doi:10.1016/j.apgeochem.2017.09.005

Feng, Y. P., Wang, G. H., Meng, Y. K., Li, D., Xu, X. M., Lu, Y., et al. (2020). Kinematics, strain patterns, rheology, and geochronology of Woka ductile shear zone: product of uplift of Gangdese batholith and Great Counter Thrust activity. *Geol. J.* 55 (11), 7251–7271. doi:10.1002/gj.3977

Gaillardet, J., Dupré, B., Louvat, P., and Allégre, C. J. (1999). Global silicate weathering and CO_2 consumption rates deduced from the chemistry of large rivers. *Chemical Geology* 159, 3–30.

Gao, W. H., Zhang, J., Zhang, W. Z., Sun, D., Guo, J. W., Zhao, S. J., et al. (2023). Hydrochemical characteristics and driving factors of travertine deposition in Huanglong, Sichuan, SW, China. *Water Sci. Technol.* doi:10.2166/wst.2023.048

Gao, Y., Li, G., Liu, Z. H., Liu, J. L., Wang, C., Xu, Z. Y., et al. (2023). Detrital zircon U-Pb isotopes and whole-rock geochemistry of early Palaeozoic sediments of the Baoshan and Lancang Blocks, SW China: implications for Proto-Tethys evolution and Gondwana reconstruction. *Geol. J.* 58, 1870–1891. doi:10.1002/gj.4697

Geng, H. P., Zhang, J., Xie, R., Dai, S. B., and Pan, B. T. (2023). The constancy of chemical weathering intensity on hillslopes in the arid to semiarid Qilian Mountains, NE Tibetan Plateau. *Sci. Total Environ.* 870, 161946. doi:10.1016/j.scitotenv.2023.161946

Gibbs, R. J. (1971). Response: mechanisms controlling world water chemistry: evaporation-crystallization process. *Science* 172 (3985), 871–872. doi:10.1126/science.170.3962.1088

Goudie, A. S., and Viles, H. A. (2012). Weathering and the global carbon cycle: geomorphological perspectives. *Earth-Science Rev.* 113 (1-2), 59–71. doi:10.1016/j.earscirev.2012.03.005

Guan, S. Z., Yang, Z., Xue, G. W., Zeng, T. G., and Yang, C. G. (1984). On the Age of the Lingxiang Formation in Southeastern Hubei and the Juro-Cretaceous Boundary. *Acta Geologica Sinica* 58, 18–26.

Guo, Y. Q., Ge, Y. G., Mao, P. N., and Liu, T. (2023). A comprehensive analysis of Holocene extraordinary flood events in the Langxian gorge of the Yarlung Tsangpo River valley. *Sci. Total Environ.* 863, 160942. doi:10.1016/j.scitotenv.2022.160942

Han, K. B., Han, Z. P., Garzanti, E., Zhu, S. P., Yao, H. W., Guo, H. F., et al. (2023). Middle Jurassic ooidal ironstones (southern Tibet): formation processes and implications for the paleoceanography of eastern Neo-Tethys. *Front. Earth Sci.* 10. doi:10.3389/feart.2022.1055957

Hemingway, J. D., Olson, H., Turchyn, A. V., Tipper, E. T., Bickle, M. J., and Johnston, D. T. (2020). Triple oxygen isotope insight into terrestrial pyrite oxidation. *Proc. Natl. Acad. Sci. U. S. A.* 117 (14), 7650–7657. doi:10.1073/pnas.1917518117

Hindshaw, R. S., Heaton, T. H. E., Boyd, E. S., Lindsay, M. R., and Tipper, E. T. (2016). Influence of glaciation onmechanisms of mineral weathering in two high Arctic catchments. *Chem. Geol.* 420, 37–50. doi:10.1016/j.chemgeo.2015.11.004

Hotelling, H. (1933). Analysis of a complex of statistical variables into principal components. *J. Educ. Psychol.* 24, 417–441. doi:10.1037/h0071325

Hren, M. T., Chamberlain, C. P., Hilley, G. E., Blisniuk, P. M., and Bookhagen, B. (2007). Major ion chemistry of the Yarlung Tsangpo-Brahmaputra river: chemical weathering, erosion, and CO2 consumption in the southern Tibetan plateau and eastern

syntaxis of the Himalaya. *Geochimica Cosmochimica Acta* 71 (12), 2907–2935. doi:10.1016/j.gca.2007.03.021

Hu, H. P., Liu, J. H., Feng, J. L., Ye, C. S., Gong, Z. J., Lv, F., et al. (2022). Geomorphic processes of a dammed palaeo-lake in the middle Yarlung Tsangpo River, Tibet. *Sci. Total Environ.* 811, 151949. doi:10.1016/j.scitotenv.2021.151949

Jia, Y. T., Kennard, M. J., Liu, Y. H., Sui, X. Y., Chen, Y. Y., Li, K. M., et al. (2019). Understanding invasion success of *Pseudorasbora parva* in the Qinghai-Tibetan Plateau: insights from life-history and environmental filters. *Sci. Total Environ.* 694, 133739. doi:10.1016/j.scitotenv.2019.133739

Jiang, L. G., Yao, Z. J., Wang, R., Liu, Z. F., Wang, L., and Wu, S. S. (2015). Hydrochemistry of the middle and upper reaches of the Yarlung Tsangpo River system: weathering processes and CO2 consumption. *Environ. Earth Sci.* 74 (3), 2369–2379. doi:10.1007/s12665-015-4237-6

Jiang, W., Ji, X., Li, Y. A., Luo, X., Yang, L. Y., Ming, W. T., et al. (2023). Modified flood potential index (MFPI) for flood monitoring in terrestrial water storage depletion basin using GRACE estimates. *J. Hydrology* 616, 128765. doi:10.1016/j.jhydrol.2022.128765

Liu, J. J., and Guo, H. C. (2023). Hydrochemical characteristics and ion source analysis of the Yarlung Tsangpo River Basin. *Water* 15 (3), 537. doi:10.3390/w15030537

Liu, W. J., Jiang, H., Zhang, J. Y., and Xu, Z. F. (2022). Driving forces of nitrogen cycling and the climate feedback loops in the Yarlung Tsangpo River Basin, the highest-altitude large river basin in the world. *J. Hydrology* 610, 127974. doi:10.1016/j.jhydrol.2022.127974

Livingstone, D. A. (1963). The sodium cycle and the age of the ocean. *Geochimica Cosmochimica Acta* 27 (Oct), 1055–1069. doi:10.1016/0016-7037(63)90066-8

Lu, P., Han, J. P., Li, Z. S., Xu, R. G., Li, R. X., Hao, T., et al. (2020). Lake outburst accelerated permafrost degradation on Qinghai-Tibet Plateau. *Remote Sens. Environ.* 249, 112011. doi:10.1016/j.rse.2020.112011

Lyu, H., Tian, F. Q., Zhang, K., and Nan, Y. (2023). Water-energy-food nexus in the Yarlung tsangpo-brahmaputra River Basin: impact of mainstream hydropower development. *J. Hydrology-Regional Stud.* 45, 101293. doi:10.1016/j.ejrh.2022.101293

Ma, Y. M., Wang, Q., Wang, H. P., Wan, B., Zhang, S. H., Deng, C. L., et al. (2022). Jurassic paleomagnetism of the Lhasa terrane-implications for tethys evolution and true polar wander. *J. Geophys. Research-Solid Earth* 127 (12). doi:10.1029/2022jb025577

Meybeck, M., Laroche, L., Durr, H. H., and Syvitski, J. P. M. (2003). Global variability of daily total suspended solids and their fluxes in rivers. *Glob. Planet. Change* 39 (1-2), 65–93. doi:10.1016/s0921-8181(03)00018-3

Millot, R., Gaillardet, J., Dupre, B., and Allegre, C. J. (2002). The global control of silicate weathering rates and the coupling with physical erosion: new insights from rivers of the Canadian Shield. *Earth Planet. Sci. Lett.* 196 (1-2), 83–98. doi:10.1016/s0012-821x(01)00599-4

Moon, S., Huh, Y., Qin, J. H., and van Pho, N. (2007). Chemical weathering in the Hong (Red) River basin: rates of silicate weathering and their controlling factors. *Geochimica Cosmochimica Acta* 71 (6), 1411–1430. doi:10.1016/j.gca.2006.12.004

Noh, H., Huh, Y., Qin, J. H., and Ellis, A. (2009). Chemical weathering in the three rivers region of eastern Tibet. *Geochimica Cosmochimica Acta* 73 (7), 1857–1877. doi:10.1016/j.gca.2009.01.005

Pearson, K. (1901). LIII. *On lines and planes of closest fit to systems of points in space. Philos. Mag.* 2 (7-12), 559–572. doi:10.1080/14786440109462720

Raymo, M. E., and Ruddiman, W. F. (1992). Tectonic forcing of late cenozoic climate. *Nature* 359 (6391), 117–122. doi:10.1038/359117a0

Ren, X. P., Nie, J. S., Saylor, J. E., Wang, X. X., Liu, F. B., and Horton, B. K. (2020). Temperature control on silicate weathering intensity and evolution of the neogene east asian summer monsoon. *Geophys. Res. Lett.* 47 (15). doi:10.1029/2020gl088808

Shan, Y. L., Zheng, H. R., Guan, D. B., Li, C. M., Mi, Z. F., Meng, J., et al. (2017). Energy consumption and CO emissions in Tibet and its cities in 2014. *Earths Future* 5, 854–864.

Stachnik, L., Majchrowska, E., Yde, J. C., Nawrot, A. P., Cichala-Kamrowska, K., Ignatiuk, D., et al. (2016). Chemical denudation and the role of sulfide oxidation at Werenskioldbreen, Svalbard. *J. Hydrology* 538, 177–193. doi:10.1016/j.jhydrol.2016.03.059

Wu, W. H. (2016). Hydrochemistry of inland rivers in the north Tibetan Plateau: constraints and weathering rate estimation. *Sci. Total Environ.* 541, 468–482. doi:10.1016/j.scitotenv.2015.09.056

Xuan, Y. X., Cao, Y. J., Tang, C. Y., and Li, M. (2020). Changes in dissolved inorganic carbon in river water due to urbanization revealed by hydrochemistry and carbon isotope in the Pearl River Delta, China. *Environ. Sci. Pollut. Res.* 27 (19), 24542–24557. doi:10.1007/s11356-020-08454-4

Yan, Y. N., Zhang, J. W., Zhang, D., Li, X. D., Wu, J., Ding, H., et al. (2022). Chemical weathering characteristics and controls in the Yarlung Tsangpo River Basin: evidence from hydrochemical composition. *Appl. Geochem.* 146, 105479. doi:10.1016/j.apgeochem.2022.105479

Yang, Y. Z., Guo, X. Y., Wu, Q. B., Jin, H. J., and Liu, F. J. (2023). Formation processes of shallow ground ice in permafrost in the Northeastern Qinghai-Tibet Plateau: a stable isotope perspective. *Sci. Total Environ.* 863, 160967. doi:10.1016/j.scitotenv.2022.160967

Yu, Z. L., Yan, N., Wu, G. J., Xu, T. L., and Li, F. (2021). Chemical weathering in the upstream and midstream reaches of the Yarlung Tsangpo basin, southern Tibetan Plateau. *Chem. Geol.* 559, 119906. doi:10.1016/j.chemgeo.2020.119906

Zhang, D. D., Peart, M., Jim, C. Y., He, Y. Q., Li, B. S., and Chen, J. A. (2003). Precipitation chemistry of Lhasa and other remote towns, Tibet. *Atmos. Environ.* 37 (2), 231–240. doi:10.1016/s1352-2310(02)00835-x

Zhang, J. W., Yan, Y. N., Zhao, Z. Q., Liu, X. M., Li, X. D., Zhang, D., et al. (2022). Spatiotemporal variation of Li isotopes in the Yarlung Tsangpo River basin (upper reaches of the brahmaputra river): source and process. *Earth Planet. Sci. Lett.* 600, 117875. doi:10.1016/j.epsl.2022.117875

Zhou, L., Xu, Z. F., Zhou, J. W., and Fan, P. K. (2022). Natural arsenic source, migration, and flux in a catchment on the Southern Tibetan Plateau. *Sci. Total Environ.* 838, 155898. doi:10.1016/j.scitotenv.2022.155898

Zhou, Z. F., Kong, J., Zhang, F. Q., Zou, Y., Xie, J. T., and Wen, C. C. (2023). Study on the carbon and nitrogen isotope characteristics and sources and their influence on carbon sinks in karst reservoirs. *Land* 12 (2), 429. doi:10.3390/land12020429